Charge Transfer Salts of Benzene-Bridged 1,2,3,5-Dithiadiazolyl Diradicals. Preparation, Structures, and Transport Properties of 1,3- and 1,4-[$(S_2N_2C)C_6H_4(CN_2S_2)$][X] (X = I, Br)

C. D. Bryan,[1a] A. W. Cordes,*[1a] R. M. Fleming,[1b] N. A. George,[1c] S. H. Glarum,[1b] R. C. Haddon,*[1b] C. D. MacKinnon,[1c] R. T. Oakley,*[1c] T. T. M. Palstra,[1b] and A. S. Perel[1b]

Contribution from the Department of Chemistry and Biochemistry, University of Arkansas, Fayetteville, Arkansas 72701, AT&T Bell Laboratories, 600 Mountain Avenue, Murray Hill, New Jersey 07974, and Guelph-Waterloo Centre for Graduate Work in Chemistry, Guelph Campus, Department of Chemistry and Biochemistry, University of Guelph, Guelph, Ontario N1G 2W1, Canada

Received February 14, 1995[⊗]

Abstract: Cosublimation of 1,3- and 1,4-benzene-bis(1,2,3,5-dithiadiazolyl) and iodine/bromine affords crystals of the mixed valence salts 1,3- and 1,4-[$(S_2N_2C)C_6H_4(CN_2S_2)$][X] (X = I, Br). The crystal structures of the two iodide salts consist of perfectly superimposed stacks of molecular units with interannular spacing along the stacks of 3.487(3) and 3.415(2) Å for the 1,3- and 1,4-derivatives. In both compounds the iodines are disordered along the stacking direction. The 1,3-derivative has a highly one-dimensional structure; there are no short intercolumnar S−S interactions. In the 1,4-derivative, however, lateral S−S contacts of 3.911 Å afford some measure of three-dimensionality. The bromide salt of the 1,4-derivative consists of ribbons of alternating 1,4-$[(S_2N_2C)C_6H_4(CN_2S_2)]^+$ units and bromide ions. Within each molecule one heterocyclic ring is closed shell, i.e., a $[CN_2S_2]^+$ cation, while the other is a discrete radical. The ribbons are layered in zigzag fashion that maximizes ion pairing and isolates the radical centers. The bromide salt of the 1,3-derivative also forms ribbon-like arrays, but the unit cell repeat consists of four layers of ribbons. Within these layers the $[CN_2S_2]$ rings are approximately stacked. The four rings within the repeat unit along each stack consists of three rings clustered into a trimeric $[CN_2S_2]_3^+$ cation, while the remaining ring is a discrete $[CN_2S_2]^+$ cation. Magnetic susceptibility and conductivity measurements on the two iodide salts indicate weakly metallic behavior at room temperature, with a charge density wave (CDW) driven metal-insulator phase transition occurring near 270 and 190 K for the 1,3- and 1,4-derivatives, respectively. For the 1,4-derivative, analysis of the CDW wavevector associated with the transition affords a degree of charge transfer of 1/4 of electron per radical, i.e., an overall formulation of $[(S_2N_2C)C_6H_4(CN_2S_2)]^{0.5+}[I]^{0.5-}$. The bromide salt of the 1,3-derivative is a closed shell insulator, while in the 1,4-bromide the isolated radical centers are antiferromagnetically coupled.

Introduction

Most molecular conductors rely on charge transfer (CT) to generate carriers. Doping can be either p-type, as in the CT salts of organic donor molecules such as TTF, TMTSF, and BEDT-TTF,[2] or n-type, as in the alkali metal salts of C_{60}.[3] For several years we have been pursuing a different approach to organic conductivity, one based on the use of neutral π-radicals, for which the requirement for a partially filled energy band is inherently fulfilled.[4] However, the exactly half-filled energy band associated with such materials is subject, in a one-dimensional packing arrangement, to a charge density wave or Peierls instability, i.e., a tendency for the radicals to dimerize. We have sought to overcome this distortion and to stabilize the metallic state (uniformly spaced radicals) by applying pressure and by preparing materials in which two- and three-dimensional interactions are enhanced. The molecular building blocks we are currently investigating are derivatives of the dithiadiazolyl radical **1** and its selenium analogue.[5] As we and others[6] have noted, the exposed peripheries of rings containing chalcogens (E = S, Se) and nitrogen are ideal for developing secondary (E−E and E−N) interactions to neighboring molecules. We have characterized the structures of a wide range of dimers **2** as a function of the substituent R-group[7] and have also pursued polyfunctional[8,9] derivatives such as the 1,3- and 1,4-benzene bridged biradicals **3**[10] and **4**.[11] Several small band gap semiconductors based on neutral selenium containing materials

⊗ Abstract published in *Advance ACS Abstracts*, June 1, 1995.

(1) (a) University of Arkansas. (b) AT&T Bell Laboratories. (c) University of Guelph.

(2) (a) Torrance, J. B. *Acc. Chem. Res.* **1979**, *12*, 79. (b) Williams, J. M.; Ferraro, J. R.; Thorn, R. J.; Carlson, K. D.; Geiser, U.; Wang, H. H.; Kini, A. M.; Whangbo, M. H. In *Organic Superconductors (Including Fullerenes): Synthesis, Structure, Properties and Theory*; Prentice-Hall, NJ, 1992. (c) Ferraro, J. R.; Williams, J. M. *Introduction to Synthetic Conductors*; Academic Press: San Diego, 1987. (d) Bryce, M. R. *Chem. Soc. Rev.* **1991**, *20*, 355.

(3) Haddon, R. C.; Hebard, A. F.; Rosseinsky, M. J.; Murphy, D. W.; Glarum, S. H.; Palstra, T. T. M.; Ramirez, A. P.; Duclos, S. J.; Fleming, R. M.; Siegrist, T.; Tycko, R. R. *Am. Chem. Soc. Symp. Ser.* **1992**, *481*, 71.

(4) Haddon, R. C. *Nature*, **1975**, *256*, 394.

(5) Cordes, A. W.; Haddon, R. C.; Oakley, R. T. In *The Chemistry of Inorganic Ring Systems*; Steudel, R., Ed.; Elsevier: 1992; p 295.

(6) (a) Zambounis, J. S.; Christen, E.; Pfeiffer J.; Rihs, G. *J. Am. Chem. Soc.* **1994**, *116*, 925. (b) Suzuki, T.; Fukui, H.; Yamashita, Y.; Kabuto, C.; Tanaka, S.; Harasawa, M.; Mukui, T.; Miyashi, T. *J. Am. Chem. Soc.* **1992**, *114*, 3034. (c) Sandman, D. J. *Mol. Cryst. Liq. Cryst.* **1979**, *50*, 235. (d) Alcock, N. W. *Adv. Inorg. Radiochem.* **1972**, *15*, 1.

(7) (a) Cordes, A. W.; Haddon, R. C.; Hicks, R. G.; Oakley, R. T.; Palstra, T. T. M. *Inorg. Chem.* **1992**, *31*, 1802. (b) Cordes, A. W.; Haddon, R. C.; Hicks, R. G.; Kennepohl, D. K.; Oakley, R. T.; Palstra, T. T. M.; Schneemeyer, L. F.; Scott, S. R.; Waszczak, J. V. *Chem. Mater.* **1993**, *5*, 820.

0002-7863/95/1517-6880$09.00/0

have been characterized, but no truly metallic compound has been realized.

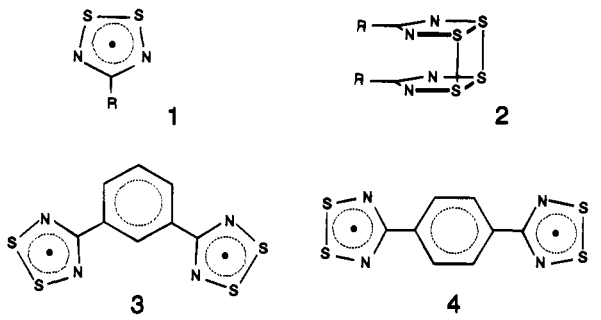

An alternative approach to stabilizing the metallic state, one which can still take advantage of the strong lateral interactions found in the neutral materials, involves p-type doping of the energy band away from the half-filled level associated with the neutral state. Recently, and in an effort to produce conductive states by doping, we reported that the triclinic phase of **1** (R = H) could be cosublimed with iodine to afford a conductive charge transfer salt of composition $[\mathbf{1}]_6[I]_{1.1}$.[12] The room temperature crystal structure of this material consists of stacks of perfectly superimposed and evenly spaced rings, and the conductivity is 15 S cm^{-1} along the needle axis. However, the volatility and air-sensitivity of this material precluded detailed transport property measurements.

Doping of the heavier, less air-sensitive benzene-bridged bis(dithiadiazolyl) radicals **3** and **4** with iodine can also be effected by cosublimation with iodine and, in a preliminary communication, we described the crystal structure and transport properties of the charge transfer salt [**4**][I].[13] We have now synthesized the bromide salts [**3**][Br] and [**4**][Br]. Herein we describe the preparation of all these mixed valence salts, i.e., [**3**][X] and [**4**][X] (X = I, Br), as well as their solid state structures and transport properties.

Results

Preparation of Mixed Valence Salts. Our initial approach to doping **3** and **4** with iodine involved sealed (*in vacuo*) tube reactions of equivalent quantities of iodine and diradical (as its dimer).[14] The two reagents were heated to about 130 °C for several hours, during which time the iodine color was slowly discharged as the CT salt was formed. Further heating of this crude material along a carefully controlled temperature gradient (180−130 °C for [**3**][I] and 220−160 °C for [**4**][I]) for 5−20 days afforded crystals of the salt as lustrous brown-black needles. Crystal twinning was a major problem which, in the case of [**4**][I], was alleviated by employing a slight overpressure (a "purple haze") of iodine. We later found that the doped materials could be conveniently prepared by heating **3** and **4** in benzonitrile or chlorobenzene in the presence of excess iodine for 1−2 h. The crude salt could be filtered off, dried *in vacuo*, and charged into a tube for purification by sublimation in a static vacuum. Sublimed crystals of [**4**][I] are indefinitely stable in air, but those of [**3**][I] slowly tarnish, either as a result of slow reaction with air or release of iodine.

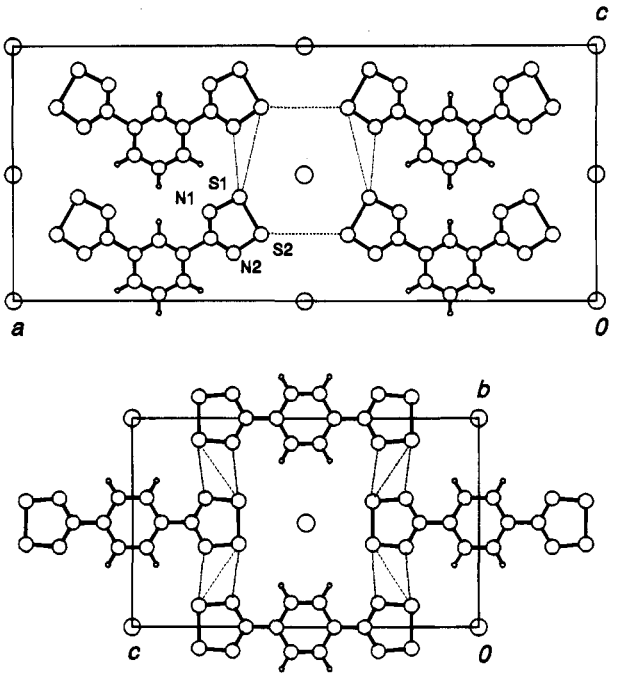

Figure 1. The "nested spoons" (above) and "dovetailed" (below) packing of [**3**][I] and [**4**][I], as viewed down the stacking direction.

The mixed valence salts [**3**][Br] and [**4**][Br] were prepared by a solid state comproportionation reaction between the native diradicals and the corresponding dibromides, i.e., $[\mathbf{3}][Br]_2$ and $[\mathbf{4}][Br]_2$. The latter were prepared by treatment of the diradicals with bromine. These reactions produce a material which, by mass balance, appears to contain significant quantities of Br_3^- ion. Excess bromine was removed from the salt by heating it *in vacuo* at 150 °C. Crystals of the mixed valence materials were grown by comproportionation of a 1:1 mixture of [**3**/**4**] and $[\mathbf{3}/\mathbf{4}][Br]_2$ in an evacuated sealed tube and subsequent sublimation along a temperature ramp of 170−130 °C (for [**3**][Br]) and 230−180 °C (for [**4**][Br]). The simple salt [**1**][Br] (R = H), whose structure was used as benchmark for a simple cation, was prepared by direct oxidation of **1** (R = H) with liquid bromine.

Crystal Structures of Mixed Valence Iodides. Full details of the structure of [**4**][I] have already been reported;[13] for comparative purposes a summary of the internal structural parameters for both [**3**][I] and [**4**][I] are listed in Table 1. Figures 1 and 2 illustrate the packing of [**3**][I] and [**4**][I], as viewed down and perpendicular to the stacking direction. Intermolecular S−S and S−N contacts for both [**3**][I] and [**4**][I] are also summarized in Table 1.

Both crystal structures are orthorhombic, belonging to the space groups *Ima*2 ([**3**][I]) and *Immm*[13,15] ([**4**][I]), and consist of columns of perfectly superimposed molecules interspersed

(8) Cordes, A. W.; Haddon, R. C.; Hicks, R. G.; Oakley, R. T.; Palstra, T. T. M.; Schneemeyer, L. F.; Waszczak, J. V. *J. Am. Chem. Soc.* **1992**, *114*, 5000.

(9) Bryan, C. D.; Cordes, A. W.; Haddon, R. C.; Hicks, R. G.; Oakley, R. T.; Palstra, T. T. M.; and Perel, A. J. *J. Chem. Soc., Chem. Commun.* **1994**, 1447.

(10) (a) Andrews, M. P.; Cordes, A. W.; Douglass, D. C.; Fleming, R. M.; Glarum, S. H.; Haddon, R. C.; Marsh, P.; Oakley, R. T.; Palstra, T. T. M.; Schneemeyer, L. F.; Trucks, G. W.; Tycko, R. R.; Waszczak, J. V.; Warren, W. W.; Young, K. M.; Zimmerman, N. M. *J. Am. Chem. Soc.* **1991**, *113*, 3559. (b) Cordes, A. W.; Haddon, R. C.; Hicks, R. G.; Oakley, R. T.; Palstra, T. T. M.; Schneemeyer, L. F.; Waszczak, J. V. *J. Am. Chem. Soc.* **1992**, *114*, 1729.

(11) Cordes, A. W.; Haddon, R. C.; Oakley, R. T.; Schneemeyer, L. F.; Waszczak, J. A.; Young, K. M.; Zimmerman, N. M. *J. Am. Chem. Soc.* **1991**, *113*, 582.

(12) Bryan, C. D.; Cordes, A. W.; Haddon, R. C.; Glarum, S. H.; Hicks, S. H.; Kennepohl, D. K.; MacKinnon, C. D.; Oakley, R. T.; Palstra, T. T. M.; Perel, A. S.; Schneemeyer, L. F.; Scott, S. R.; Waszczak, J. V. *J. Am. Chem Soc.* **1994**, *116*, 1205.

(13) Bryan, C. D.; Cordes, A. W.; Fleming, R. M.; George, N. A.; Glarum, S. H.; Haddon, R. C.; Oakley, R. T.; Palstra, T. T. M.; Perel, A. S.; Schneemeyer L. F.; Waszczak, J. V. *Nature* **1993**, *365*, 821.

(14) Hilti, B.; Mayer, C. W. *Helv. Chim. Acta* **1978**, *63*, 501.

(15) Unit cell parameters for [4][I]: a = 3.415(2), b = 10.061(2), c = 16.740(2) Å, Z = 2.

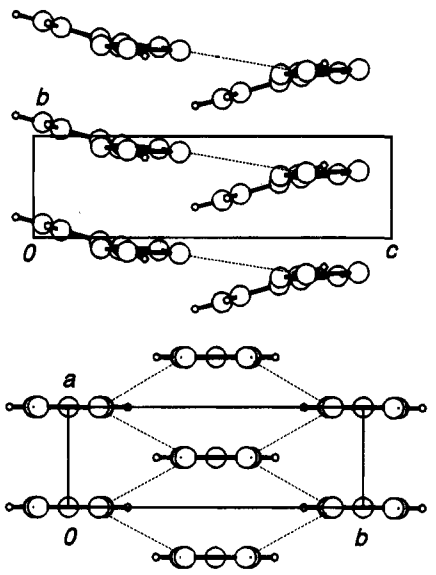

Figure 2. Stacking of [3][I] (above) and [4][I] (below), showing weak intermolecular S−S contacts. The disordered iodines have been omitted for clarity.

Table 1. Summary of Mean Intra- and Intermolecular Distances (Å) in [4][I] and [3][I][a]

	[3][I]		[4][I]
	Intramolecular		
S−S	2.067(13)		2.067(1)
S−N	1.616(21)		1.616(1)
C−N	1.30(4)		1.337(3)
	Intermolecular		
S2−S2′	4.300(10)	S−S′	3.911(1)
S1−S2′	4.530(15)	S−N′	3.320(2)
S1−N2′	3.558(20)		

[a] Numbers in parentheses are the greater of the ESD and range.

by columns of iodines. The heterocyclic rings are evenly spaced at 3.487(3) and 3.415(2) Å, respectively. These distances are longer than the mean close interannular S−S separations of 3.140 and 3.121 Å in the neutral compounds $[3]_2$ and $[4]_2$.[10,11] In contrast to [4][I], in which the molecule is bisected by three mutually perpendicular mirror planes, the structure of [3][I] lies on a single mirror plane that bisects the benzene ring. As a whole the molecule is far from planar; the plane of the two CN_2S_2 rings makes a dihedral angle of 14.3° with that of the benzene ring. This deviation from planarity is partly a result of the "nested spoons" packing arrangement of the molecules in the *z* direction. The benzene rings are accordingly forced to twist away from an orientation which would accentuate repulsive CH−HC, CH−N, and CH−S contacts. In both [3][I] and [4][I] the iodine atoms are disordered along the stacking direction. In both structures the disorder was modeled by three fractional iodines, with the dominant site being in the plane of the two adjacent heterocyclic rings. This "head-on" mode of coordination of a halide to the two sulfurs of a dithiadiazolium cation has been observed elsewhere[16,17] and is found exclusively in the bromide salts described below.

In contrast to the four-fold pinwheel patterns found in the solid state structure of $[3]_2$, the "nested spoons" packing motif of [3][I] leads to an extremely one-dimensional electronic structure; there are no short interstack S−S contacts that would foster the development of a more two- or three-dimensional electronic structure. For example, the closest intercolumnar contact is the head-to-head S2−S2′ distance which, at 4.300(10) Å, is well outside the standard van der Waals contact[18] for two sulfurs (3.60 Å). The closest contact in the *z* direction, S1−S2′ (4.530(15) Å), is even longer. The S1−N2′ distance (3.558(20) Å) is also well outside the sum (3.35 Å) of the van der Waals radii for S and N. The dovetailed packing observed in [4][I] affords better lateral approaches, and both S−S′ (3.911(1) Å) and S−N′ (3.320(2) Å) are significantly closer than in [3][I], although still not as close as seen in the neutral dimer $[4]_2$.

Table 2. Summary of Intra- and Intermolecular Distances (in Å) in [1][Br], [4][Br], and [3][Br]

[1][Br] (R = H)		[4][Br]		[3][Br]	
		Intramolecular			
S1−S2	2.011(3)	S1−S1	2.007(4)	S5−S6	2.004(9)
S1−N1	1.577(7)	S1−N1	1.593(5)		
S2−N2	1.593(7)	N1−C1	1.326(6)	S1−S2	2.020(8)
N1−C1	1.332(13)			S3−S4	2.076(8)
N2−C1	1.319(13)	S2−S2′	2.076(4)	S7−S8	2.071(8)
		S2−N2	1.637(5)		
		N2−C6	1.348(6)		
		Intermolecular			
				S1−S7	3.258(9)
				S2−S8	3.294(9)
				S3−S8	3.012(9)
				S4−S7	2.946(9)
Br−Br′	4.203(2)	Br−Br	4.487(1)	Br1−Br1′	4.172(6)
Br′−Br′	4.537(1)			Br1−Br2	5.171(5)
				Br2−Br2′	4.356(8)
S1−Br	3.119(2)	S1−Br	3.112(2)	S5−Br1	3.043(7)
S2−Br	3.081(2)	S2−Br	3.342(2)	S6−Br1	3.151(8)
S1−Br′	3.281(3)	S1−Br[a]	3.323(2)	S5−Br1′	3.042(8)
S2−Br′	3.353(3)	S1−Br[a]	4.045(2)		
S1′−Br′	3.370(3)			S1−Br2	3.108(6)
S2′−Br′	3.641(3)	S1−S2′	3.849(3)	S2−Br2	2.949(6)
		S2−S2′	3.678(4)	S3−Br2	3.116(7)
				S4−Br2	3.238(7)
				S7−Br2	3.344(6)
				S8−Br2	3.409(7)

The degree of charge transfer in the two structures can be assessed in a qualitative way by comparison of the internal structural parameters, notably the S−S and S−N bond lengths, with those found in related compounds. As has been discussed elsewhere,[19−21] the singly occupied molecular orbital (SOMO) of dithiadiazolyl radicals is antibonding with respect to both the S−S and S−N linkages. Accordingly, these bonds undergo a slight but predictable contraction as the oxidation state of the CN_2S_2 ring changes from zero to +1. In both [3][I] and [4][I] the observed S−S and S−N distances are intermediate between those found in fully oxidized materials, e.g., $[4][SbF_6]_2$, and the neutral dimers $[3]_2$ and $[4]_2$. Overall the balance slightly favors the latter and suggests an oxidation state of <+0.5 for each ring.

Crystal Structure of [1][Br]. Crystals of [1][Br] (R = H) belong to the monoclinic space group $P2_1/a$, with $Z = 4$; a summary of pertinent intra- and intermolecular distances is provided in Table 2. The structure consists of antiparallel ribbons of bromide anions and $[HCN_2S_2]^+$ cations (see Figure 3). As expected, the intramolecular bond lengths are all typical

(16) Bryan, C. D.; Cordes, A. W.; Haddon, R. C.; Hicks, R. G.; Oakley, R. T.; Palstra, T. T. M.; Perel, A. S.; Scott, S. R. *Chem. Mater.* **1994**, *6*, 508.

(17) Hazell, A.; Hazell, R. G. *Acta Crystallogr.* **1988**, *C44*, 1807.

(18) Bondi, A. *J. Phys. Chem.* **1964**, *68*, 441.

(19) Cordes, A. W.; Bryan, C. D.; Davis W. M., DeLaat, R. H.; Glarum, S. H.; Goddard, J. D.; Haddon, R. C.; Hicks, R. G.; Kennepohl, D. K.; Oakley, R. T.; Scott S. R.; Westwood, N. P. C. *J. Am. Chem. Soc.* **1993**, *115*, 7232.

(20) Banister, A. J.; Hansford, M. I.; Hauptman, Z. V.; Luke, A. W.; Wait, S. T.; Clegg, W.; Jørgenson, K. A. *J. Chem. Soc., Dalton Trans.* **1990**, 2793.

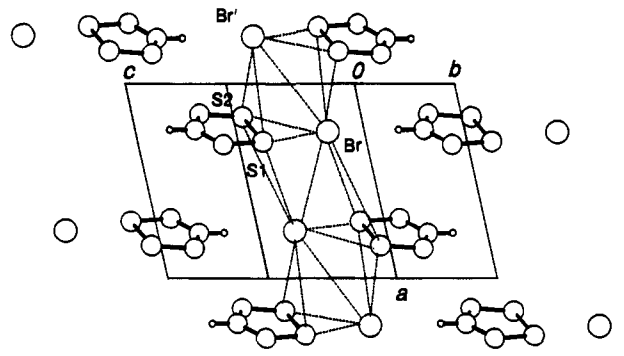

Figure 3. Antiparallel layers of bromide anions and $[HCN_2S_2]^+$ cations in [**1**][Br] (R = H). Close S−Br contacts are shown with dashed lines.

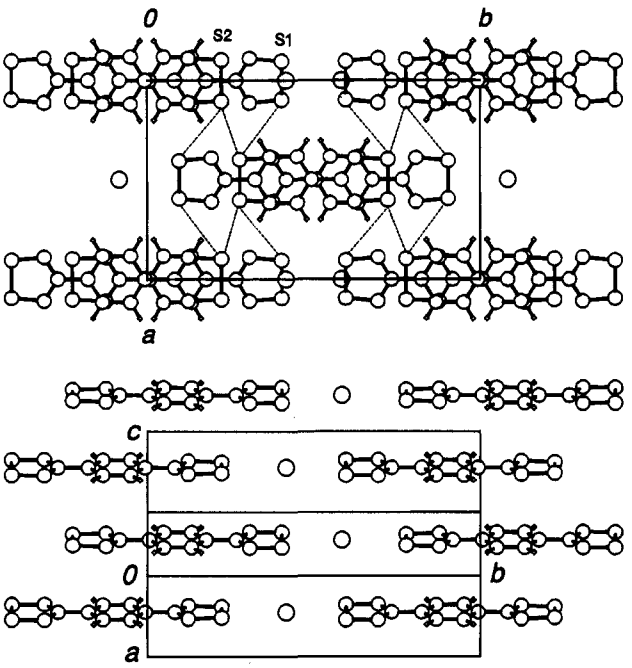

Figure 4. Ribbon-like packing of [**4**][Br] in the *xy* plane (above) and offset layering of ribbons along *z*.

for the +1 oxidation state of the HCN_2S_2 heterocycle.[19,21] Ion pairing forces hold the bromide ions in a tight pocket, with one cation ring bound "head-on" (*via* S1−Br and S2−Br interactions) and two others situated above and below the bromide (the S1/S2−Br/Br′ and S1′/S2′−Br′ contacts) (see Table 2 and Figure 3). The remaining coordination site on bromine is taken up by a weak H−Br interaction (2.797(1) Å). At 4.203(2) Å (Br−Br′) and 4.537(1) Å (Br′−Br′) the bromide ion separations are outside the sum of the ionic radii (for six-coordinate bromide $r(Br^-)$ = 1.82 Å).[22]

Crystal Structure of Mixed Valent Bromides. Crystals of [**4**][Br] belong to the monoclinic space group *C*2/*c*; a summary of pertinent intra- and intermolecular distances is provided in Table 2. The crystal structure consists of ribbon-like arrays of alternating $[\mathbf{4}]^{\cdot+}$ radical cations and bromide anions strung together along two-fold axes running parallel to the *y* direction; these ribbons form in-register layers in the *xy* plane, as shown in Figure 4. The ribbons are layered in the *z* direction, each layer being offset from the one above and below so that the halide ion of one layer is approximately aligned with the internal S−S bond of one of the CN_2S_2 rings in the layers above and below it. This packing arrangement, which is similar to that

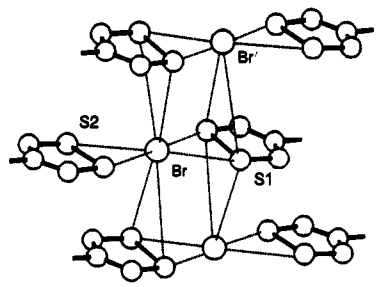

Figure 5. The coordination shell of the bromide ions in [**4**][Br].

described above for [**1**][Br], affords a zigzag stacking of bromides ions in the *z* direction, with a Br−Br separation (4.487(1) Å) intermediate between the two values noted above for [**1**][Br]. The coordination shell for each bromide ion consists of four "head-on" CN_2S_2 rings (Figure 5). Two of these are in-plane (contacts S1/S2−Br) and two are out-of-plane contacts (S1′/S2′−Br). The inequivalence in the latter two distances arises from the slight rotation of the molecules about the two-fold symmetry axis. The differences in the S1/S2−Br contacts, however, reflect the important electronic differences in the two in-plane rings (hereafter termed the S1 and S2 rings). As the internal structural parameters in Table 2 indicate, the S1 ring, which is "sandwiched" between two bromides above and below, displays S−S and S−N distances which are consistent with a fully oxidized cation. The S2 ring, by contrast, which takes the coordination site occupied by the Br−HC contact in [**1**][Br], has internal S−S and S−N distances which indicate a free radical or zero oxidation state. There are no close (inside or near van der Waals') S−S contacts between these radical rings and those in the ribbons above and below. As illustrated in Figure 4, there are lateral, in-register contacts (S1−S2′) between radical and cationic rings in adjacent ribbons; there are also out-of-register contacts (S2−S2′) between adjacent neutral rings.

Crystals of [**3**][Br] belong to the monoclinic space group $P2_1/c$; a summary of pertinent intra- and intermolecular distances is provided in Table 2. There are two radical cation molecules (and two Br^- ions) in the asymmetic unit, with $Z = 4$. The structure consists of "S-shaped" ribbons composed of alternating molecules of $[\mathbf{3}]^+$ and bromide ions; this unit snakes its way across the unit cell in the *z* direction (Figure 6). The layering of these ribbons is more complex than in the [**4**][Br] structure. When viewed down the *x* direction, the layered ribbons take on a corrugated, pseudo-stacked appearance (Figure 6). The spacing of the ribbons, however, is by no means uniform, indeed the repeat distance along the *y* direction consists of four layers, as expected from the degree of bandfilling (*vide infra*). The layers are built about shallow zigzag stacks of bromide ions. Within these stacks (Figure 7) the Br^-−Br^- separations (Br1−Br1, Br1−Br2′, Br2−Br2′, see Table 2) vary widely. The Br1 bromides are coordinated to a free-standing cation (the S5/S6 ring). The latter is also coordinated (*via* the S5−Br1′ contact) to a bromide below it. The Br2 bromides are more heavily coordinated. Each is encapsulated by four rings, two S7/S8 and one each of S1/S2 and S3/S4 (see Table 2). Collectively the six rings which cluster around the two bromides form two closed-shell triple-decker $[CN_2S_2]_3^+$ units reminiscent of those observed in the mixed valence salts $[PhCN_2S_2]_3[I_3]$ **5**[16] and $[PhCN_2S_2]_6[Cl]_2$ **6**,[23] where the oxidation state of each ring is formally +1/3. The internal S−S and S−N distances in the present cluster, and also the long interannular S−S bonds, are analogous to those observed in the latter two species. In the case of **5** the electronic structure of the molecular unit has been

(21) Cordes, A. W.; Goddard, J. D.; Oakley, R. T.; Westwood, N. P. C. *J. Am. Chem. Soc.* **1989**, *111*, 6147.
(22) Shannon, R. D. *Acta Crystallogr.* **1976**, *A32*, 751.
(23) Banister, A. J.; Howard, J. A. K.; Lawrence, S. E. *Phosphorus, Sulfur and Silicon* **1994**, *93/94*, 437.

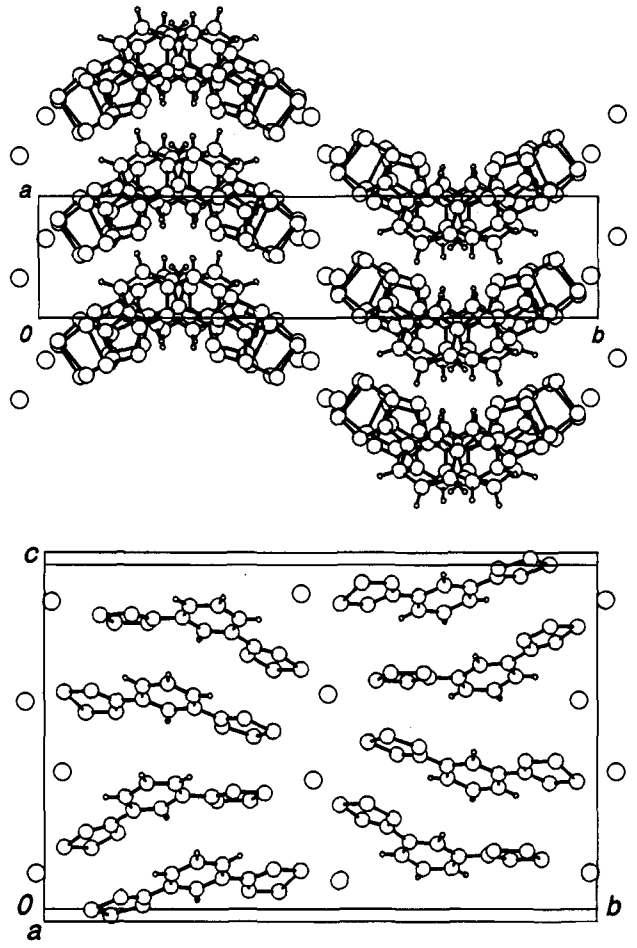

Figure 6. Snake-like ribbons of [3][Br] (above) and corrugated layering of ribbons (below).

described in terms of a pseudo-allyl cation, with two π^*-electrons binding the three-ring sequence together.[16]

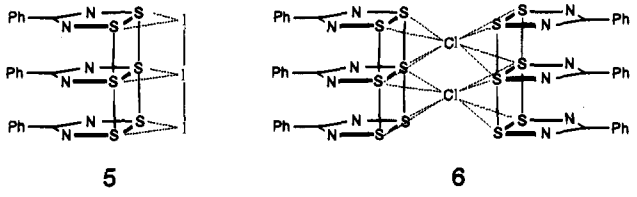

5 6

Superlattice Measurements. Low temperature X-ray diffraction experiments on [4][I] revealed the presence of a superlattice.[13] This superlattice, the formation of which is reversible, was discovered by taking scans parallel to the stacking directon $[h,0,0]$ at several points in reciprocal space. This approach was based on the assumption that a CDW should have at least one component along the direction of highest conductivity. Scans along $[h,0,6]$ revealed small superlattice peaks at $h = \pm 3/8$ and $h = \pm 6/8$ around the $[0,0,6]$ Bragg reflection. The third harmonic at $h = 9/8$ was not observed, nor was the Bragg reflection at $[1,0,6]$, which is absent because of the body-centered lattice. Similar superlattice peaks were observed around nearly every major Bragg reflection in the $(0,k,l)$ zone but were not observed along $[0,0,l]$. The onset of the superlattice reflections is near 200K, in agreement with the magnetic and conductivity data (*vide infra*), and is interpreted as arising from a charge density wave with $\mathbf{q} = (3/8)\mathbf{a}^*$, where $\mathbf{a}^*$ is the reciprocal lattice vector. The CDW wavevector is apparently commensurate at $h = 3/8$ at all temperatures in the range 10−300 K, but the low q-resolution may have prevented the detection of a region of incommensurability near the phase transition.

Table 3. Crystal Data

compound	[3][I]	[1][Br] (R = H)	[4][Br]	[3][Br]
formula	$C_8H_4N_4S_4I$	CHN_2S_2Br	$C_8H_4N_4S_4Br$	$C_8H_4N_4S_4Br$
fw	411.29	185.06	364.29	364.29
a, Å	28.12(1)	7.0375(7)	10.553(9)	5.649(4)
b, Å	3.487(3)	8.375(3)	16.382(3)	25.777(2)
c, Å	12.28(2)	8.883(2)	7.113(2)	16.560(9)
β, deg	103.58(2)	112.13(6)	95.79(5)	
V, Å^3	1204(2)	508.9(2)	1139(1)	2399(2)
d(calcd), g cm^{-3}	2.27	2.415	2.12	2.02
space group	*Ima*2	*P*21/*a*	*C*2/*c*	$P2_1/c$
Z	4	4	4	8
λ, Å	0.71073	0.71073	0.71073	0.71073
temp, K	293	293	293	293
μ, mm^{-1}	3.28	8.63	4.26	4.04
$R(F^2)$, $R_w(F^2)^a$	0.057, 0.081	0.043, 0.064	0.033, 0.075	0.074, 0.103

$^a R = [\sum||F_o| - |F_c||]/[\sum|F_o|]$; $R_w = \{[\sum w||F_o| - |F_c||^2]/[\sum(w|F_o|^2)]\}^{1/2}$.

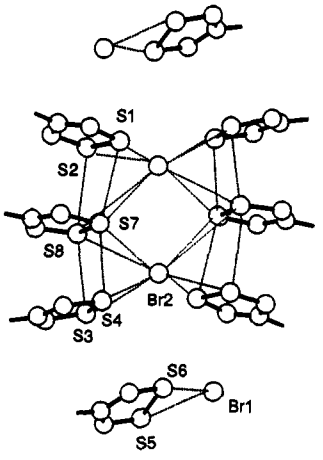

Figure 7. Coordination shells of bromide ions in [3][Br].

Magnetic Measurements. Figure 8 shows the magnetic susceptibility behavior of [3][I] and [4][I] as a function of temperature. As noted previously for [4][I] the materials are basically diamagnetic insulators at low temperatures. A Curie fit to the data below 100 K leads to susceptibilities of −166 and −149 cgs ppm/mol for the diamagnetic terms for [3][I] and [4][I], in good agreement with estimates based on the Pascal scheme. The concentrations of unpaired spins are found to be 0.13% and 0.01%, respectively. At increased temperatures paramagnetism develops in both materials. This rise begins near 250 K in the case of [3][I] and (more sharply) at 200 K for [4][I]. It is interesting to note that a paramagnetic transition of about the same magnitude also occurs in neutral $[3]_2$ but at a temperature of 450 K. However, this latter transition does not contribute appreciably to the conductivity. Figure 9 shows the magnetic susceptibility behavior of [4][Br] as a function of temperature. In the high temperature regime the compound shows strong paramagnetism, with a Curie susceptibility corresponding to almost one unpaired spin per molecule; antiferromagnetism, however, develops below room temperature. The compound undergoes a phase transition at 15 K which quenches the magnetism. This magnetic quenching is presumably associated with a dimerization process, as observed in the neutral radicals. However, since the radicals are unable to dimerize in the conventional cofacial manner, other interactions, such as the lateral S2−S2′ contacts noted earlier, must be involved.[24] The driving force for dimerization in [4][Br] would thus be

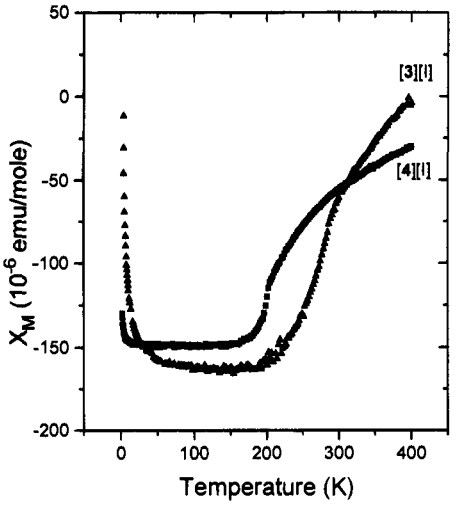

Figure 8. Magnetic susceptibility of [3][I] and [4][I] as a function of temperature.

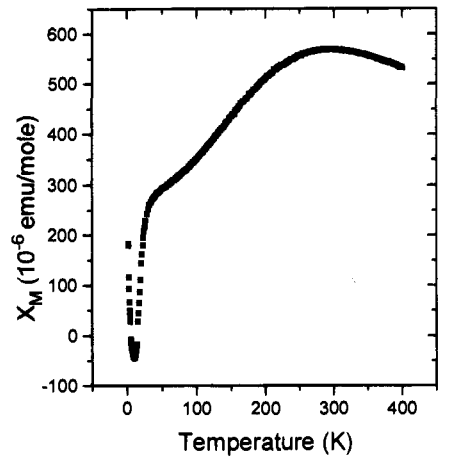

Figure 9. Magnetic susceptibility of [4][Br] as a function of temperature.

expected to be quite weak because of the poor overlap between radical centers.

Conductivity Measurements. Single crystal conductivities (along the needle axis) of both [3][I] and [4][I] are shown in Figure 10 as a function of temperature. The results show that the transitions seen in the magnetic measurements correspond to metal-insulator transitions. For both compounds the conductivity is activated in the low temperature region; above 210 K for [4][I] and above 300 K for [3][I] the conductivity is weakly metallic. The highest conductivities attained are 100 S cm^{-1} for [4][I] at *ca.* 350 K and 20 S cm^{-1} for [3][I] at *ca.* 400 K. The application of about 1 Gpa pressure increased the conductivity of [3][I] and [4][I] by about a factor of 4 but did not appreciably suppress the metal-insulator transitions. The larger size and quality of [4][I] have allowed us to perform variable temperature conductivity measurements along all three principal crystal directions; Figure 11 shows the results of these experiments. In all three directions the same features, as a function of temperature, are observed. The ordering of the conductivities, with $\sigma_a > \sigma_b > \sigma_c$, is as expected, but the anisotropies (100:25:1) suggest relatively strong lateral interactions.

(24) Isolated dithiadiazolyl radicals have also been observed in the recently reported structure of **1** (R = NCC_6F_4). Aherne, C. M.; Banister, A. J.; Bricklebank, N.; Clegg, W.; Elsegood, R. J.; Gregory, C. I.; Howard, J. A. K.; Lavender, I.; Lawrence, S. E.; Rawson, J. M.; Tanner, B. K. *J. Chem. Soc., Chem. Commun.* **1995**, 679.

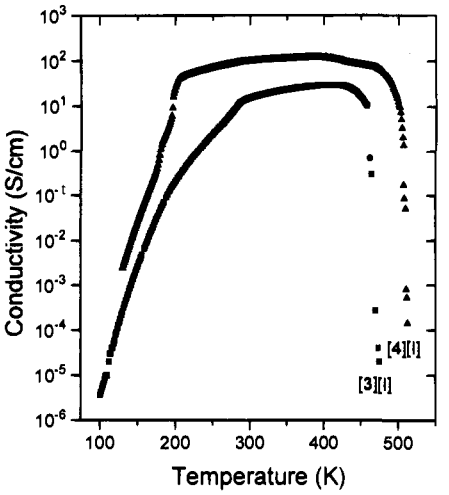

Figure 10. Conductivity of [3][I] and [4][I] as a function of temperature.

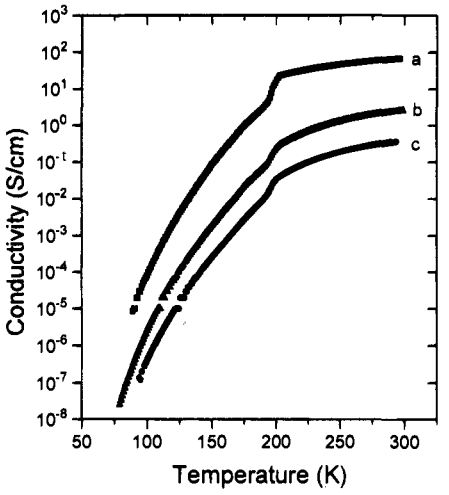

Figure 11. Conductivity of [4][I] along the three principal crystal directions.

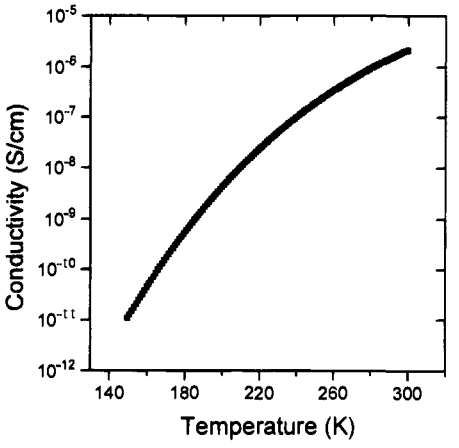

Figure 12. Conductivity of [4][Br] as a function of temperature.

The bromide salts are poor conductors. Conductivity measurements (Figure 12) confirm [4][Br] as an antiferromagnetic insulator, while the closed shell compound [3][Br] has a pressed pellet conductivity (room temperature) of 10^{-5} S cm^{-1} (similar to that observed for **5**).[22]

The above results can be compared with the structures and transport properties of charge transfer complexes of other organosulfur compounds with halogens.[25,26] Tetrathiafulvalene (TTF), for example, forms a wide range of salts of formula

$[TTF][X]_y$ (X = I, Br, Cl). All the phases, regardless of the nature of X, with $0.7 < x < 0.8$ show a similar stacking arrangement, with separate ordered, incommensurate sublattices for the TTF and halogen columns.[27] There are no close lateral intercolumnar S—S contacts, and the variations in the stoichiometries depend on the electronegativity and size of the halogen. Integral oxidation states, e.g., [TTF][Br] and [TTF][Cl], are also known, but these consist of arrays of $[TTF]_2^{2+}$ dimers and counterions; these salts are not conductive. The stacked salts, which are highly one-dimensional, show activated conductivity at low temperature, with a "flat" conductivity regime above a transition temperature of 230 K for X = I and 180 K for X = Br.[28] Tetrathiatetracene (**TTT**) also forms a series of CT salts with halogens, some of which (notably $[TTT]_2[I_3]$ or $[TTT][I]_{0.75}$) are highly conductive with a metallic temperature dependence to below 100 K. The structure of $[TTT]_2[I_3]$ consists of slipped stacks of $[TTT]^+$ cations and chains of disordered triiodide anions running parallel to the *y* direction (cell repeat, $b = 3.32(2)$ Å). The **TTT** molecules are oriented in rows along the *z* direction, with close interannular "head-on" contacts (3.373(2) Å) between sulfur atoms on neighboring rings. Presumably the latter impart some degree of two-dimensionality to the structure. There are no short S-halogen contacts, as found in the $[TTF][X]_y$ materials.[29,31]

By comparison with the TTF and TTT salts, localized cation—anion interactions appear to dominate the structures of [**3**][X] and [**4**][X] (X = I, Br); the "head-on" coordination mode $[CN_2S_2]$—X is a common feature of all the structures. Such heavy ion pairing is not found in either the TTF or TTT salts, although it has been observed in some CT salts of tetraselenatetracene.[31] The exact 1:1 stoichiometry of the stacked dithiadiazolyl structures reflects the importance of these local ion-pairing interactions.

Discussion

In our previous studies of dithia- and diselenadiazolyl radicals, we have noted the inevitable tendency of the radical stacks to collapse into stacked dimers. This CDW-driven or Peierls distortion opens up an energy gap at the Fermi level, and the materials are, at best, small band gap semiconductors. Our objective in preparing mixed valence salts of dithiadiazolyl radicals has been to shift the electronic structure away from the half-filled energy band associated with the neutral radicals (Figure 13) and to generate a degree of bandfilling which is no longer commensurate with a simple dimerization process. However, regardless of the degree of charge transfer, and the consequent level of bandfilling, CDW-driven lattice distortions can still occur. The structures reported here provide appealing examples.

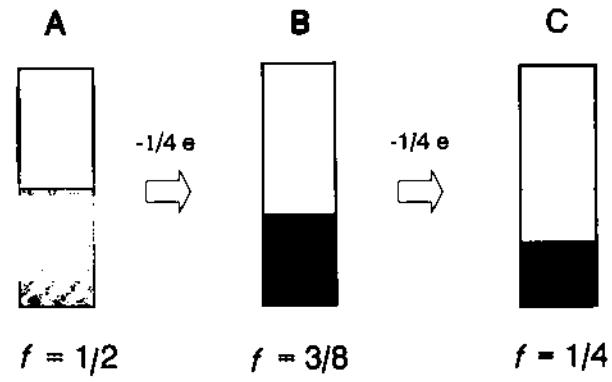

Figure 13. Degree of band filling (*f*) in neutral (A), 1/4+ charged (B), and 1/2+ charged (C) stacks of [**1**].

Low temperature X-ray diffraction experiments of [**4**][I] show the presence of a superlattice with wavevector $\mathbf{q} = (3/8)\mathbf{a}^*$.[13] We previously used this result to establish the degree of charge transfer. The analysis assumes that the observed distortion correponds to twice the Fermi wavevector, $\mathbf{q} = 2\mathbf{k}_F$, in which case $\mathbf{q} = \varrho\mathbf{a}^*/2$, where ϱ is the average number of carriers per lattice site.[32] For a nondegenerate band, ϱ is twice the degree of bandfilling (*f*). Thus, in the case of [**4**][I], we argued that the superlattice implies that $\varrho = 3/4$ and $f = 3/8$, and a depletion by 1/4e of the conduction band associated with the neutral state (Figure 13), or a formulation of $[\mathbf{4}]^{+0.5}[I]^{-0.5}$ and a formal charge of +1/4 per CN_2S_2 ring. We have no clear indication as to the nature of the iodine based species, although a mixture of iodide (I^-) and triiodide (I_3^-) ions readily accounts for the formal charge.

In a further development of this analysis we construct a simple model of the low temperature CDW state of [**4**][I]. Let the translation vector of a molecule [**4**] in the high temperature structure be given by $\mathbf{r} = l\mathbf{a} + m\mathbf{b} + n\mathbf{c}$, where **a**, **b**, and **c** are the direct space lattice vectors, and *l*, *m*, and *n* are integers. In the presence of a harmonic modulation along **a** with wavevector **q**, the displacements Δr will be given by eq 1 (in which *A* and ϕ are the amplitude and phase).

$$\Delta \mathbf{r} = A \sin(\mathbf{q}\cdot\mathbf{r} + \phi) \tag{1}$$

$$= A \sin[(3/8)\mathbf{a}^*\cdot l\mathbf{a} + \phi] \quad [\text{for } \mathbf{q} = (3/8)\mathbf{a}^*,\ l = 1, 2, 3 \ldots]$$

$$= A \sin[2\pi(3/8)l + \phi]$$

These displacements correspond to the simplest periodic lattice distortion necessary to open a gap at the Fermi level, where $\mathbf{q} = 2\mathbf{k}_F$, the Fermi wavevector.[33] Note that the function is periodic over (8/3)**a**, but only commensurate with the original lattice when taken over eight unit cells along **a**. In the classical case of a half-filled energy band $\mathbf{q} = (1/2)\mathbf{a}^*$, and the lattice distortions generate a sequence of dimers, as illustrated in Figure 14, i.e., the lattice repeat is doubled from **a** to **2a**. Such is the fate of the neutral dithia- and diselenadiazolyl radicals we have studied to date. In the 1:1 charge transfer iodide [**4**][I], however, $\mathbf{q} = (3/8)\mathbf{a}^*$, and the superlattice consists of the eight-tier array shown in Figure 14.

It is immediately and strikingly obvious that the metallic lattice $[CN_2S_2]_8^{2+}$ collapses into a series of discrete, *chemically recognizable* units, i.e., a triple decker cation $[CN_2S_2]_3^+$, a simple cation $[CN_2S_2]^+$, and two neutral dimers $[CN_2S_2]_2$; all

(25) Marks, T. J.; Kalina, D. W. In *Extended Linear Chain Compounds*; Miller, J. S., Ed.; Plenum Press: New York, 1982; pp 197—331.

(26) Coppens, P. In *Extended Linear Chain Compounds*; Miller, J. S., Ed.; Plenum Press: New York, 1982; pp 333—356.

(27) (a) Scott, B. A.; LaPlaca, S. J.; Torrance, J. B.; Silverman, B. D.; Welber B. *J. Am. Chem. Soc.* **1977**, *99*, 6631. (b) Gane, P. A. C.; Kathirgamamanathan, P.; Rosseinsky, D. R. *J. Chem. Soc., Chem. Commun.* **1981**, 378. (c) Kathirgamanamanathan, P.; Rosseinsky, D. R. *J. Chem. Soc., Chem. Commun.* **1980**, 356.

(28) (a) Warmack, R. J.; Callcott, T. A.; Watson; C. R. *Phys. Rev.* **1975**, *12B*, 3336. (c) Sonwoano, R. B.; Gupta, A.; Hadek, V.; Datta, T.; Jones, R.; Herman, A. M. *J. Chem. Phys.* **1975**, *63*, 4970.

(29) (a) Buravov, L. I.; Zvereva, G. I.; Kaminskii, V. F.; Rosenberg, L. P.; Khidekel, M. L.; Shibaeva, R. P.; Shchegolev, I. F.; Yagubskii, E. B. *J. Chem. Soc., Chem. Commun.* **1976**, 720. (b) Kaminskii, V. F.; Khidekel, , M. L.; Lyubovskii, R. B.; Shchegolev, I. F.; Shibaeva, R. P.; Yagubskii, E. B.; Zvargina, A. V.; Zverena, G. L. *Phys. Status Solidi* **1977**, *44A*, 77.

(30) Smith, D. L.; Luss, H. R. *Acta Crystallogr.* **1977**, *33B*, 1744.

(31) Delhaes, P.; Coulon, C.; Flandrois, S.; Hilti, B.; Mayer, C. W.; Rivory, J. *J. Chem. Phys.* **1980**, *73*, 1452.

(32) (a) Whangbo, M.-H. In *Crystal Chemistry of Materials with Quasi-One Dimensional Structures*; Rouxel, J., Ed.; D. Reidel Publishing Co.: Dordrecht, 1986; p 27. (b) Canadell, E.; Whangbo, M.-H. *Chem. Rev.* **1991**, *91*, 965.

(33) (a) Kagoshima, S.; Nagasawa, H. Sambongi, T. In *One-dimensional Conductors*; Springer Verlag: New York, 1982. (b) Rouxel, J. In *Crystal Chemistry of Materials with Quasi-One Dimensional Structures*; Rouxel, J., Ed.; D. Reidel Publishing Co.: Dordrecht, 1986; p 1.

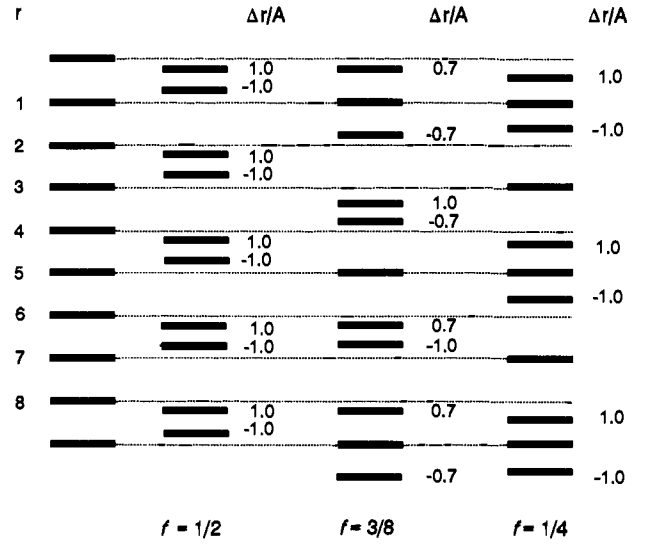

Figure 14. Periodic lattice displacements ($\Delta r/A$) of a one-dimensional stack for different degrees of bandfilling f. The value of the weighting factor A is a function of the CDW. For ease of comparsion the phase factor ϕ is set equal to $\pi/2$ for $f = 1/2$ and to zero for $f = 3/8$ and 1/4.

are closed-shell. The simple sinusoidal modulation expected from eq 1 not only opens a gap at the Fermi level but also imposes distortions of the lattice that are in good accord with previous structural precedents. For example, the displacements necessary to make dimers within this array are, as expected, greater than those required to generate the trimer cations. Placed within a chemical context, the interannular S−S contacts in the dimer units are expected to be slightly smaller than the corresponding S−S distances in the trimer cations. Such a prediction is entirely in accord with experiment; values of 3.10 Å for intradimer S−S spacings are typical, while the intratrimer S−S spacings in **5** are 3.18 Å (mean value). Further analysis of the model allows us to anticipate large separations between monomers and dimers and even larger dimer to trimer separations. Nevertheless, it should be noted that the appearance of a harmonic at $\mathbf{q} = (6/8)\mathbf{a}^*$ may indicate that higher order structural distortions are important in defining the final lattice positions. Clearly, all the clusters are closed-shell units, and the bulk material is likewise diamagnetic. If the same CDW model is applicable to [**3**][I], the higher onset temperature for the metal-insulator transition presumably originates from the lower dimensionality of this material.

In the bromide salts the presence of discrete, well-ordered bromide ions heralds a formal charge of, on average, +1/2 per CN_2S_2 per ring. A perfectly superimposed stacked structure, however, is not observed in [**4**][Br], indeed the ionic radius of Br^- is too large to allow it. Instead the structure contains one radical ring (0 charge) and one cation (+1 charge) per molecular unit. While the array of radicals is nominally associated with a half-filled energy band, the weakness of the radical−radical interactions (only the lateral S2−S2′ contacts) is such that an antiferromagnetic structure prevails. The seemingly complex structure of [**3**][Br], with stacked arrays of triple-decker $[CN_2S_2]_3^+$ cations and $[CN_2S_2]^+$ cations, is most easily interpreted in terms of a severe CDW associated with a 1/4-filled energy band (Figure 13).[32] Application of the above analysis to such a system, with $\mathbf{q} = (1/4)\mathbf{a}^*$, reveals a plate distortion pattern completely consistent with the observed structure (Figure 14). The displacements cause three rings to cluster tightly together, i.e., to form a closed-shell $[CN_2S_2]_3+$ cation, while one remains isolated as a discrete $[CN_2S_2]^+$ cation. The magnitude of the distortion is such that the resulting material is a rather poor conductor, even at room temperature.

In summary, the susceptibility of stacked dithiadiazolyl CT salts to undergo well defined structural distortions finds a simple explanation in terms of the strong, localized S−S interannular S−S interactions known to occur in neutral dimers and trimer cations. Closed-shell structures exhibiting semiconducting or insulating behaviour are thus easily accessible by charge density waves. While the rather high MI transition temperature of 270 K in [**3**][I] is not unexpected, given the paucity of short lateral S−S contacts, the high value for T_{MI} in [**4**][I] is surprising in the light of the observed anisotropies (100:25:1), which indicate well-developed lateral interactions. By comparison, in TMTSF salts such as $(TMTSF)_2ClO_4$, the conductivity anisotropies (at room temperature) are 900:40:1.[34] The variations in anisotropy observed between [**3**][I] and [**4**][I] encourages exploration of other bifunctional dithiadiazolyl CT salts. If lateral interactions can be further enhanced, a metallic ground state may prevail. We are also examining other charge transfer acceptors for use in conjunction with dithiadiazolyl radicals, and extending the chemistry to include selenium as well as sulfur based radicals.

Experimental Section

Starting Materials and General Procedures. Iodine (Fisher) and bromine (Aldrich) were obtained commercially; iodine was resublimed before use. Benzonitrile (Aldrich) was purified by distillation from P_2O_5. The dithiadiazolyl radical **1** (R = H)[20] and the diradicals **3**[1,3] and **4**[1,4] were prepared according to literature methods and the dimers purified by vacuum sublimation. All reactions (in solution) were carried out under an atmosphere of nitrogen. The doping and comproportionation reactions were performed in an ATS series 3210 three-zone tube furnace, linked to a series 1400 temperature control system. Elemental analyses were performed by MHW Laboratories, Phoenix, AZ. Infrared spectra of the bromide salts were recorded (at 2 cm^{-1} resolution) on a Nicolet 20SX/C infrared spectrometer. IR spectra of the iodide salts could not obtained because of excessive scattering of the incident radiation by the sample.

Sealed Tube Preparation of [3][I] and [4][I]. Equimolar quantities of the dimer of **3** or **4** (284 mg, 0.500 mmol) and I_2 (126 mg, 0.500 mmol) were sealed in an evacuated (10^{-3} Torr) pyrex tube (25 mm × 250 mm). The tube was then placed in a three-zone tube furnace with all three zones set at 130 °C. Over a period of several hours the initially intense purple color faded as the iodine was adsorbed by the dimer to generate the CT salt. The temperature along the tube was then ramped, from 180 to 130 °C for [**3**][I] and from 220 to 160 °C for [**4**][I], and the assembly left for a period ranging from 5 to 20 days. Crystals of the iodide salts slowly grew in the cooler regions of the tube. Yields were as high as 80%, although values of 40−50% were more typical. The crystals were harvested in air but were stored under argon. [**3**][I] grows as flat, brown/black needles, while [**4**][I] forms more rodlike needles (also brown/black). Anal. Calcd for $C_8H_4N_4S_4I$: C, 23.96; H, 0.98; N, 13.62; I, 30.86. Found (for [**3**][I]): C, 23.25; H, 1.06; N, 13.34; I, 31.05. Found (for [**4**][I]): C, 23.56; H, 0.85; N, 13.62; I, 30.98.

Solution Preparation of [3][I] and [4][I]. Samples of the dimer of **3** or **4** (284 mg, 0.500 mmol) and excess iodine (*ca.* 0.3 g) in 20 mL benzonitrile were heated to 130 °C for 2 h in a sealed Schlenk tube. The mixture was then cooled, and the CT salt filtered off, washed with CH_3CN, and pumped dry. The crude materials (black powders) so obtained (yields 85% for [**3**][I] and 100% for [**4**][I]) were purified by gradient sublimation as described above.

Preparation of [1][Br] (R = H). The dimer of **1** (R = H, 0.20 g, 0.95 mmol) and bromine (0.20 g, 1.1 mmol) were added separately to the two halves of an evacuated H-cell. The bromine was then transfered *in vacuo* to the radical-containing arm, and the vessel allowed to warm to room temperature. The crystalline solid so obtained was recrystallized twice from liquid SO_2 as bright red blocks (recrystallized yield 0.23 g, 1.2 mmol, 63%), dec > 200 °C. Infrared spectrum (1600−200 cm^{-1}) 1264 (s), 943 (w), 848 (m), 821 (s), 815 (s), 802 (vs), 561(s),

(34) Murata, K.; Anzai, H.; Saito, G.; Kajimura, K.; Ishiguro, T. *J. Phys. Soc. Jpn.* **1981**, *50*, 3529.

529(m) cm^{-1}. Anal. Calcd for CHN_2S_2Br: C, 6.49; H, 0.54; N, 15.14; Br, 43.18%. Found: C, 6.39; H, 0.77, N, 15.26; Br, 43.46%.

Preparation of [3][Br]$_2$ and [4][Br]$_2$. The dimer of **3** or **4** (0.284 g, 0.500 mmol) was slurried together with an excess of bromine (0.2 g) in dry CH_3CN (10−15 mL). The slurry was heated (with vigorous stirring) at 65 °C for 45 min during which time a bright red precipitate was formed. After cooling the solution to room temperature, the solid was filtered off, washed with CH_3CN, and pumped dry for several hours. Excess bromine (trapped as a tribromide) was removed by heating the crude solid at 150 °C under dynamic vacuum for several hours. Yields of the crude dibromides were 95−100%.

Preparation of [4][Br]. The dimer of **4** (0.284 g, 0.500 mmol) was combined with crude [**4**][Br]$_2$ (0.364 g, 1.00 mmol) in a sublimation tube (25 mm × 250 mm). The tube was evacuated to 2.0×10^{-3} Torr, sealed, and placed in a furnace at a uniform temperature of 180 °C. After 1 h the temperature was increased to 230 °C, and the material was left overnight. The following day the tube was cooled and opened, and the black solid transferred to a new sublimation tube, which was then evacuated and sealed as before. This tube was then placed back in the furnace and the temperature along the tube ramped from 230 to 180 °C. Sublimation (1−2 days) yielded lustrous black crystalline blocks. Yields varied between 75 and 150 mg: mp >350 °C; IR spectrum (1600−200 cm^{-1}) 1009 (m), 920 (w), 894 (s), 845 (s), 825 (s), 803 (s), 685 (s), 651 (m), 551 (m), 508 (s). Anal. Calcd for $C_8H_4N_4S_4Br$: C, 26.38; H, 1.11; N, 15.38; Br, 21.93. Found: C, 26.57; H, 1.26; N, 15.45; Br, 21.71.

Preparation of [3][Br]. The dimer of **3** (0.284 g, 0.500 mmol) was combined with crude [**3**][Br]$_2$ (0.364 g, 1 mmol) in a sublimation tube (25 mm × 250 mm). The tube was evacuated to 2.0×10^{-3} Torr, sealed, and placed in a furnace at a uniform temperature of 170 °C. The following day the tube was cooled and opened and the black solid was transferred to a new sublimation tube, which was then evacuated and sealed as before. This tube was replaced into the furnace, and the temperature along the tube ramped from 170 to 130 °C. Sublimation (2−12 days) yielded lustrous black crystalline blocks. Yields varied between 75 and 150 mg: mp 158−165 °C; IR spectrum (1600−200 cm^{-1}) 1352 (m), 1289 (m), 1167 (w), 1115 (w), 973 (m), 881 (w), 828 (m), 795 (m), 723 (m), 690 (m). Anal. Calcd for $C_8H_4N_4S_4Br$: C, 26.38; H, 1.11; N, 15.38; Br, 21.93. Found: C, 26.14; H, 0.96; N, 15.20; Br, 22.14%.

X-ray Measurements. All X-ray data were collected on an ENRAF-Nonius CAD-4 diffractometer with monochromated Mo Kα (λ = 0.71073 Å) radiation. Crystals were mounted on a glass fiber with epoxy or silicone. Data were collected using a $\theta/2\theta$ technique. The structures were solved using direct methods and refined by full-matrix least squares which minimized $\sum w(\Delta F)^2$. A summary of crystallographic data is provided in Table 3. As with other systems of this type, the crystals of [**3**][I] readily twin; the data set used for this report is one of three complete data sets collected; at least 10 different crystals were actually mounted on the diffractometer in order to find those with minimal twinning. The extent of twinning of the crystals was also observed on Weissenberg photographs. The relatively high *R*-value for [**3**][Br] is ascribed to lack of crystal quality (as shown by the high *R*-merge for averaging duplicate reflections) and the paucity of data because of the small crystal size, which precluded anisotropic refinement of the C and N atoms.

Superlattice Measurements. Low temperature X-ray diffraction was performed on a single crystal of [**4**][I] by using a Cu K_α rotating-anode detecting source and a closed-cycle helium refrigerator. A singly-bent pyrolytic graphite monochromator and a flat graphite analyzer were used to increase the signal-to-noise ratio and minimize scattering from the cryostat Be windows. This arrangement resulted in a symmetric resolution function with a resolution width of about 0.01 $Å^{-1}$.

Magnetic Susceptibility Measurements. The magnetic susceptibilities as a function temperature were measured using a SQUID magnetometer operating at 1 Tesla.

Conductivity Measurements. Four-point conductivity measurements along the highly conducting axes were performed with a Keithley 236 unit. Gold pads were first evaporated onto some of the crystals. For low temperature experiments the wires were attached to the pads with gold paint. For high temperature measurements silver paint was used, as it proved more durable at elevated temperatures. Due to the irregularities of the sample the conductivity of [**4**][Br] was determined with a two-point measurement. Given the low conductivity of this material, the contact resistance may be neglected.

Acknowledgment. Financial support at Guelph was provided by the Natural Sciences and Engineering Research Council of Canada (NSERC) and at Arkansas by the National Science Foundation (EPSCOR program). C.D.B. acknowledges a DOE/ASTA Traineeship, and C.D.M. an NSERC postgraduate scholarship.

Supporting Information Available: Tables of crystal data, structure solution and refinement, atomic coordinates, bond lengths and angles, and anisotropic thermal parameters for [**3**][I], [**1**][Br] (R = H), [**3**][Br], and [**4**][Br] (12 pages). This material is contained in many libraries on microfiche, immediately follows this article in the microfilm version of the journal, can be ordered from the ACS, and can be downloaded from the Internet; see any current masthead page for ordering information and Internet access instructions.

JA950522S